AD-A123 659 ENERGY SCALING LAWS FOR THE RACETRACK INDUCTION ACCELERATOR(U) NAVAL RESEARCH LAB WASHINGTON DC A A MONDELLI ET AL. 29 DEC 82 NRL-MR-5008 1/1

UNCLASSIFIED F/G 20/7 NL

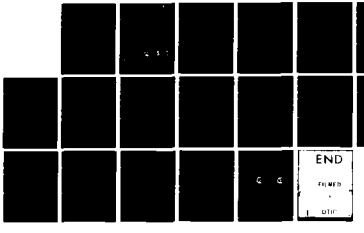

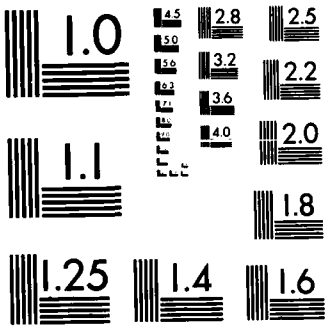

NRL Memorandum Report 5008

Energy Scaling Laws for the Racetrack Induction Accelerator

A. A. MONDELLI

Science Applications, Inc.
McLean, VA 22102

C. W. ROBERSON

Plasma Physics Division

December 29, 1982

NAVAL RESEARCH LABORATORY
Washington, D.C.

SECURITY CLASSIFICATION OF THIS PAGE (When Data Entered)

REPORT DOCUMENTATION PAGE		READ INSTRUCTIONS BEFORE COMPLETING FORM
1. REPORT NUMBER NRL Memorandum Report 5008	2. GOVT ACCESSION NO. AD-A123 659	3. RECIPIENT'S CATALOG NUMBER
4. TITLE (and Subtitle) ENERGY SCALING LAWS FOR THE RACETRACK INDUCTION ACCELERATOR		5. TYPE OF REPORT & PERIOD COVERED Final report on an NRL problem. 6. PERFORMING ORG. REPORT NUMBER
7. AUTHOR(s) A. A. Mondelli* and C. W. Roberson		8. CONTRACT OR GRANT NUMBER(s)
9. PERFORMING ORGANIZATION NAME AND ADDRESS Naval Research Laboratory Washington, DC 20375		10. PROGRAM ELEMENT, PROJECT, TASK AREA & WORK UNIT NUMBERS 61153N; RR0110941; 47-1484-0-2
11. CONTROLLING OFFICE NAME AND ADDRESS Office of Naval Research Arlington, VA 22217		12. REPORT DATE December 29, 1982 13. NUMBER OF PAGES 30
14. MONITORING AGENCY NAME & ADDRESS(if different from Controlling Office)		15. SECURITY CLASS. (of this report) Unclassified 15a. DECLASSIFICATION/DOWNGRADING SCHEDULE
16. DISTRIBUTION STATEMENT (of this Report) Approved for public release; distribution unlimited.		
17. DISTRIBUTION STATEMENT (of the abstract entered in Block 20, if different from Report)		
18. SUPPLEMENTARY NOTES *Science Applications, Inc. McLean, VA 22102		
19. KEY WORDS (Continue on reverse side if necessary and identify by block number)		

20. ABSTRACT (Continue on reverse side if necessary and identify by block number)

A high-current, cyclic electron accelerator, capable of accelerating several kiloamperes of electron current is described. The accelerating elements of the device are linear induction modules, which match well to high-current operation. A racetrack configuration is utilized to return the electrons to the induction modules, thereby providing electron acceleration to an energy given by the gap voltage multiplied by the number of electron transits during the total pulse duration of the induction modules.

(Continued)

DD FORM 1 JAN 73 1473 EDITION OF 1 NOV 65 IS OBSOLETE
S/N 0102-014-6601

SECURITY CLASSIFICATION OF THIS PAGE (When Data Entered)

20. ABSTRACT (Continued)

The bends are stabilized against toroidal drifts due to field curvature and gradients by imposing an l = 2 stellarator field to average the drift motion. This field is analogous to an alternate gradient focussing field. It provides containment of particles up to a maximum energy, E_{max}, above which the orbits become too large to fit within the toroidal chamber. For a 10 cm diameter chamber on a 1 meter radius bend, the maximum energy is approximately 1 MeV per kilogauss of guide field. For a 3 meter bend, E_{max} = 2.3 MeV/kG. This scaling sets an upper limit of $\lesssim$ 50 MeV for this configuration, before the size and/or field required becomes excessive.

To move beyond this limit, a vertical magnetic field may be utilized to cancel the toroidal forces at a particular energy. This field must be increased as the particles are accelerated. In this configuration, the stellarator windings provide a tolerance in the allowed mismatch between the vertical field and the particle energy. Electron energies up to ~ 1 GeV can be achieved in this configuration.

CONTENTS

ENERGY SCALING LAWS FOR THE RACETRACK INDUCTION ACCELERATOR

I. INTRODUCTION

Particle accelerators have been developed as low current, high energy machines, or as low voltage and high current devices such as Marx-pulse line systems. Induction accelerators have the potential of both high current and high voltage operation.

In this paper, the energy scaling laws of the Racetrack Induction Accelerator[1] (RIA) are determined and its operating principles are discussed. This device is a cyclic accelerator that is capable of high current operation. Long pulse induction linac technology is used to obtain short acceleration times. The RIA circulates a high current beam through a linear induction module. The voltage gain relation is $V = V_M T_M/\tau$, where V_M is the voltage gain per pass, T_M is the module pulse duration and τ is the transit time of the beam around the accelerator. One of the potential applications of a high current, high voltage accelerator is to drive free electron lasers (FEL). The wavelength scales as

$$\lambda = \lambda_w/2\gamma^2$$

where γ is the relativistic factor and λ_w the wiggler wavelength. The minimum practical values of λ_w are about 1 cm. Therefore beam voltages in excess of 50 MeV are required to produce visible radiation.

High current free electron lasers have the potential of compact and efficient operation. High current free electron lasers at wavelengths less than 1 mm operate in the kinetic Compton regime.[2] The growth rate is proportional to the slope of the distribution function. The FEL is driven only by the beam particles in resonance with the pondermotive wave of the FEL. Saturation occurs in the FEL because of nonlinear modification of the resonant particles. In the racetrack a mechanism such as pitch angle scattering due to field errors can be sufficient to restore the beam. The time scale for this modification should be comparable with the transit time around the accelerator. Although the gain may not be large, the efficiency can be high. This is a potential advantage of a racetrack over a linear accelerator for driving a FEL.

At the present time the linear induction accelerator is the most common high voltage and high current system in existence. Typically, iron or ferrite-core induction acceleration modules are matched at a beam current of 1-2 kA. To achieve particle acceleration to high energy is mainly a matter of length and cost. Accelerating gradients are typically 0.5 MeV/m, with some designs reaching as high as 1.0 MeV/m. The size of these machines implies large cost and requires large commitments of real estate. Costs in excess of $1/Volt are now common. Very high current linear induction accelerators are possible through the use of radial pulselines to drive the accelerating gaps, as has been shown in the RADLAC[3] accelerator at Sandia National Laboratories.

Various folded or cyclic accelerator designs have been proposed and studied in an effort to achieve high voltage and high current systems without the huge cost and space requirements of the induction linac. A conventional betatron, for example, is current limited at injection, when the energy is low and the betatron fields are too small to contain the beam space charge. A betatron with a high-energy injector has been studied at Livermore and Berkeley in an effort to overcome the space-charge limit. A

Manuscript approved November 12, 1982.

more radical modification to the betatron, the so-called modified betatron, is under study at the Naval Research Laboratory[4] and at U.C. Irvine.[5] In this approach a toroidal magnetic field is used to contain the space charge at early times in the accelerating cycle. The need for high-energy injection, and a costly pre-accelerator, is thereby removed.

One approach for utilizing a linear induction accelerator to reach high energy is the recirculating linac concept,[6] which has been studied at the National Bureau of Standards. In this approach, the accelerator is in fact a folded linac, with the total charge carried through a linear induction module several times. On each transit the beamlets are enclosed by drift tubes, which isolate them from each other while passing through the module. Since each induction module can accommodate only a small number of these drift tubes, modules must be stacked to reach high voltage. The racetrack induction accelerator, which is the subject of this report, is in fact a cyclic accelerator, in which the entire beam current circulates around a racetrack, passing through linear induction modules on the straight legs of the racetrack.

The racetrack induction accelerator, shown schematically in Fig. 1-1, consists of a long-pulse ($\sim$2 μs) linear induction module and a racetrack beam transport system which allows the electron beam to be returned to the linear induction module. A high-current electron beam requires an axial magnetic guide field for stable propagation. The minimum guide field for equilibrium is given by

$$B = \left(\frac{8\pi^2 nmc^2}{\gamma} \right)^{1/2},$$

where n is the beam number density. For a 1 kA/cm^2 beam current density and 1 MeV electrons, this criterion gives $B > 2.4$ kG. Higher fields will be required in the bends to control drift orbits and may also be required to suppress resonant instabilities. In the bends the curvature and gradient in the guide field leads to a vertical drift of the particle orbit. By adding a uniform vertical magnetic field (perpendicular to the plane of the orbit), the resulting Lorentz force can be made to cancel the centrifugal and grad B forces at a particular electron energy, thereby removing the vertical drift. To maintain an equilibrium as the particles are accelerated, the vertical field must be synchronous with the acceleration of the beam. Since the acceleration occurs only in the induction module, the vertical field at the input and output of the module must be different, thereby forcing a spatially-dependent field. This solution is very sensitive to the accuracy to which the vertical magnetic field can be made synchronous with the acceleration. Small field errors can result in rapid loss of the particle.

The poor stability of the vertical field solution is due to its requirement of exact, local force cancellation at a particular energy. Instead, it is possible to design a magnetic field configuration which provides cancellation of the spatially averaged force felt by an electron in the bend over a band of particle energies. This configuration is provided by a quadrupole field which is twisted into a helix, as in an $l = 2$ stellarator. The helical field causes the particle to circulate about the minor axis of the bend, so that in drifting vertically, it drifts toward the axis for half the time in the bend and away from the axis for the other half. The net effect of this motion is to average the net drift displacment to zero. All particles with energies up to some maximum are contained within this field configuration. Very energetic particles will have drift orbits which are too large to fit within the minor cross-section of the device, and will therefore not be contained. The stellarator winding in conjunction with the long-pulse induction module makes a fixed-field accelerator up to the maximum particle energy. Since the focussing and confining fields can be independent of time, the pulse shape of the induction module can be arbitrary.

To accelerate particles to energies in excess of the maximum contained in a fixed-field system, a time-dependent vertical magnetic field may be employed on the bends, as described above. In this configuration, having combined vertical and stellarator fields, the time-independent stellarator component provides an energy bandwidth of approximately the maximum energy of the fixed-field system, thereby relaxing the requirements on the vertical field in matching the particle energy in both space and time.

These two configurations allow two classes of accelerators to be identified. The fixed-field configuration is best suited for accelerating a multi-kiloamp beam to modest energies (up to 50 MeV). The combined vertical and stellarator field configurations is a high-energy system, capable of reaching energies up to 1 GeV.

II. FIXED-FIELD RACETRACK INDUCTION ACCELERATOR

In conventional, low-current cyclic accelerators the bending magnetic fields must be synchronous with the particle energy. To contain the space charge in a high-current accelerator requires an axial magnetic field, which introduces curvature and grad B drifts. These drifts can be canceled by imposing a vertical magnetic field which is made synchronous with the particle acceleration. Unlike a conventional accelerator, where an asynchronism in the bending field causes the particle to adjust its radial equilibrium position, an asynchronism in the vertical field of a high-current accelerator causes a vertical displacement which offers no new equilibrium.

In place of the vertical field, a twisted quadrupole field provides a cancellation of the average force felt by a particle in traversing a bend. This technique avoids the problems of field synchronism because the particle drifts average to zero for all energies below a maximum. The bending and confining fields in this case are independent of time. The twisted quadrupole configuration is analogous to an alternate-gradient strong-focussing system. This configuration, including the axial magnetic field, is an $l = 2$ stellarator field, which was designed to control particle drifts in magnetic confinement fusion.[7,8]

Near the magnetic axis of a cylindrical helix, the field has a remarkably simple structure, which may be used to study the drift motion of a charged test particle. Toroidal effects may be included to the simplest approximation by imposing a gravitational-type of curvature drift due to the centrifugal force. The magnetic field is given by

$$B_x = b\alpha y \cos 2\alpha z - b\alpha x \sin 2\alpha z$$

$$B_y = b\alpha x \cos 2\alpha z + b\alpha y \sin 2\alpha z$$

$$B_z = B_0 + 0(b\alpha^2 r^2)$$

where x, y, z are a right-handed coordinate system having the z-axis aligned with the cylinder axis. When toroidal curvature is included, it is assumed to add a force acting in the x-direction. The fields above are valid for $2\alpha r \ll 1$ and $b\alpha r \ll B_0$. B_0 is the solenoidal field amplitude, while b is the amplitude of the helical field, and $\alpha \equiv 2\pi/L$ where L is the pitch length of the helix.

The following drifts are constructured:

- Gradient-B Drift

$$\underline{V}_g = -\frac{c}{2}\frac{\gamma m v_\perp^2}{qB}\frac{\nabla B \times \underline{B}}{B^2}$$

- Drift Due to the Lorentz Force

$$\underline{V}_F = \frac{1}{B^2}(\underline{v} \times \underline{B}) \times \underline{B}$$

- Curvature Drift

$$\underline{v}_c = \frac{\gamma m v_\parallel^2 c}{qRB^2}\hat{e}_x \times \underline{B}$$

where $q \equiv -|e|$ and $v_\perp^2$, $v_\parallel^2$ are relative to $\underline{B}$, but are approximately $v_\parallel^2 = v_z^2$ and $v_\perp^2 = v_x^2 + v_y^2$ for $B_0 >> b\alpha r$. The transverse components of these drifts may be written as

$$\underline{v}_{g\perp} = -\eta(-y\hat{e}_x + x\hat{e}_y)$$

$$\underline{v}_{F\perp} = \beta[\hat{e}_x(y\cos 2\alpha z - x\sin 2\alpha z) + \hat{e}_y(x\cos 2\alpha z + y\sin 2\alpha z)]$$

$$\underline{v}_{c\perp} = -\hat{e}_y\beta y_*,$$

where

$$\eta \equiv -\frac{\gamma m v_\perp^2 c b^2 \alpha^2}{2qB_0^3}$$

$$\beta \equiv \frac{v_\parallel b\alpha}{B_0}$$

$$y_* \equiv \frac{\gamma m v_\parallel c}{qRb\alpha}.$$

The total transverse drift vector, $\underline{v}_D = \underline{v}_{g\perp} + \underline{v}_{F\perp} + \underline{v}_{c\perp}$, is therefore

$$V_{Dx} = \eta y + \beta y\cos 2\alpha z - \beta x\sin 2\alpha z$$

$$V_{Dy} = -\eta x + \beta x\cos 2\alpha z + \beta[y\sin 2\alpha z - y_*].$$

The equilibrium position of the particle under these drifts is given by $(\bar{x}(z), \bar{y}(z))$ which force $\underline{v}_D = 0$,

$$\bar{x}(z) = -\frac{\beta y_*}{\eta^2 - \beta^2}(\eta + \beta\cos 2\alpha z)$$

$$\bar{y}(z) = -\frac{\beta y_*}{\eta^2 - \beta^2}(\beta\sin 2\alpha z).$$

As it moves along the z-axis, the projection of the equilibrium orbit on the x-y plane is a circle of radius, $\beta^2 y_*/(\eta^2 - \beta^2)$, whose center is displaced from the geometric axis by a distance, $-\eta\beta y_*/(\eta^2 - \beta^2)$, in the x direction.

The stability of this drift equilibrium may be studied by examining displacements from this equilibrium. Define $\tilde{x} = x - \bar{x}$ and $\tilde{y} = y - \bar{y}$. Then

$$\frac{d\tilde{x}}{d\xi} = -(\tilde{\beta}\sin\xi)\tilde{x} + (\tilde{\eta} + \tilde{\beta}\cos\xi)\tilde{y}$$

$$\frac{d\tilde{y}}{d\xi} = -(\tilde{\eta} - \tilde{\beta}\cos\xi)\tilde{x} + (\tilde{\beta}\sin\xi)\tilde{y},$$

where $\xi = 2\alpha z$, $\tilde{\beta} = \beta/2\alpha v_\parallel$ and $\tilde{\eta} = \eta/2\alpha v_\parallel$.

For $\tilde{\eta} = 0$, which corresponds to $v_\perp = 0$, a particularly simple solution is possible for a quadrupole field with no twist, oriented as though $\sin(2\alpha z) = 1$ everywhere. In this case, the solution is

$$\tilde{x}(\xi) = \tilde{x}_0 e^{-\tilde{\beta}\xi}$$

$$\tilde{y}(\xi) = \tilde{y}_0 e^{+\tilde{\beta}\xi},$$

which is stable in the x-direction and unstable in the y-direction, with the growth (damping) increment given by $\tilde{\beta}$, which is $b/2B_0$. In the opposite limit, where α is large, so that the helical field varies with a scale length that is short compared to the growth length, the equations for x and y can be averaged over the helical period to yield

$$\tilde{x}(\xi) \sim e^{\pm i\tilde{\eta}\xi}$$

$$\tilde{y}(\xi) \sim e^{\pm i\tilde{\eta}\xi}$$

which are oscillatory. Twisting the quadrupole field therefore has the effect of averaging the drifts that were introduced by the axial magnetic field.

When $\tilde{\eta} = 0$, the shift in the equilibrium position for the particle is given by y_*,

$$y_* = \frac{\gamma m v_{\|} c}{qRb\alpha} = \frac{\gamma c}{\Omega_c} \cdot \frac{v_{\|}}{c} \cdot \frac{1}{\tilde{\beta}} \cdot \frac{1}{2\alpha R}$$

which should be small compared with the minor radius of the bend, and smaller than the separatrix of the stellarator field. Here, $\Omega_c \equiv qB_0/mc$ is the nonrelativistic cyclotron frequency.

The differential equations for $\tilde{x}(\xi)$ and $\tilde{y}(\xi)$ have been solved numerically, with $\tilde{\eta} << \tilde{\beta}$ for the initial condition $\tilde{x}(0) = -y_*$ and $\tilde{y}(0) = 0$, which corresponds to a particle which starts on the magnetic axis. Since the equations for $\tilde{x}$ and $\tilde{y}$ are homogenous, the initial condition can be scaled out of the problem with the transformation

$$\delta x = \tilde{x}/y_*$$

$$\delta y = \tilde{y}/y_*.$$

δx and δy satisfy the same differential equations as $\tilde{x}$ and $\tilde{y}$, and the initial conditions are $\delta x(0) = -1$ and $\delta y(0) = 0$.

Figure 2-1 shows the result of this integration as $x(\xi)$ vs $y(\xi)$, where

$$x(\xi) = \bar{x}(\xi)/y_* + \delta x(\xi)$$

$$y(\xi) = \bar{y}(\xi)/y_* + \delta y(\xi),$$

for $\tilde{\eta} = -.001$ and for $\tilde{\beta}$ varied from 0.1 to 0.5. The equilibrium orbit, $\bar{x}(\xi)/y_*$ vs $\bar{y}(\xi)/y_*$, is plotted as a heavy circle on each figure. The orbits are stable for $\tilde{\beta} < 0.5$. The $\tilde{\beta} = 0.5$ trajectory increases monotonically in amplitude, as seen in Fig. 2-2, which shows $\delta x(\xi)$ vs $\delta y(\xi)$. This case, $\tilde{\beta} = 0.5$, corresponds to $b = B_0$, at which point the separatrix collapses onto the magnetic axis, as will be seen below, for an $l = 2$ stellarator.

For detailed studies of the particle dynamics in a racetrack, a numerical model is required to integrate the fully-relativistic single-particle equations of motion,

$$\frac{d}{dt}(\gamma m \underline{v}) = -\frac{e}{c}\,\underline{v} \times \underline{B},$$

where $\gamma = (1 - v^2/c^2)^{-1/2}$ and $\underline{B}$ is the externally applied magnetic field. The actual structure of $\underline{B}(\underline{x})$ may be found in several ways, but the first approach has been to use an analytical approximation for the field.

The magnetic scalar potential for a toroidal stellarator field, to first order in the inverse aspect ratio, is given by[9]

$$\begin{aligned}\Phi_l(r, \theta, s) = B_0\Bigg\{ & s + \frac{\epsilon_l}{\alpha} I_l(x) \sin[l(\theta - \alpha s)] \\ & - \frac{k\epsilon_l}{4l\alpha^2}[x^2 I_l'(x) - x(1 + l) I_l(x)] \sin[(l + 1)\theta - l\alpha s] \\ & - \frac{k\epsilon_l}{4l\alpha^2}[x^2 I_l'(x) - x(1 - l) I_l(x)] \sin[(l - 1)\theta - l\alpha s] \\ & + \frac{\epsilon_{l+1}^*}{\alpha} I_{l+1}(x) \sin[(l + 1)\theta - l\alpha s]\end{aligned}$$

$$+ \frac{\epsilon_{l-1}^*}{\alpha} I_{l-1}(x) \sin [(l-1)\theta - l\alpha s] \Bigg\},$$

where $x = l\alpha r$, $\alpha = 2\pi/L$, L is the pitch length of the helical field, $k = 1/R_0$, and R_0 is the major radius of the torus. $\epsilon_{l\pm1}^*$ is given by

$$\epsilon_{l\pm1}^* = \frac{k\epsilon_l}{\alpha} \left[\frac{\epsilon_{l\pm1}}{\epsilon_l} + \frac{x_0^2}{4} \right],$$

$$\frac{\epsilon_{l\pm1}}{\epsilon_l} = \frac{1}{4K_l(x_0)} [K_{l\pm1}(x_0) - x_0 K_{l\pm1}'(x_0)],$$

where $x_0 = l\alpha r_0$ and r_0 is the minor radius of the helical current sheet which generates the field. A more general form of the potential would consist of a summation over the l-number. The numerical work described here has been carried out entirely for the $l = 2$ stellarator field. The parameter, ϵ_l, measures the relative strength of the helical and solenoidal field contributions. The helical field strength, b, in the analytical theory described above is simply $b = \epsilon_l B_0$.

The magnetic field is found from this scalar potential by taking the toroidal gradient,

$$B_r = \frac{\partial \phi_l}{\partial r}$$

$$B_\theta = \frac{1}{r} \frac{\partial \phi_l}{\partial \theta}$$

$$B_s = (1 - kr \cos\theta) \frac{\partial \phi_l}{\partial s},$$

to first order in kr.

The straight sections are modeled as regions of pure solenoidal field, $B_r = B_\theta = 0$, $B_z = B_s = B_0$. The toroidal stellarator field is assumed to apply over the entire bend, which is modeled as a semicircular region. A region of straight section adjacent to each end of the bends is used to force a transition from a solenoidal to a stellarator field configuration. If the transition occurs in the regions $s_1 \leqslant s \leqslant s_2$, the prescription followed is

$$\epsilon_l(s) = \epsilon_l \left[1 - \frac{s - s_1}{s_1 - s_2} \right]$$

$$k(s) = k \left[1 - \frac{s - s_1}{s_2 - s_1} \right]$$

in order to linearly remove the helical and toroidal field contributions. Other model transitions, such as parabolic and cosine, have also been tried with no effect on the particle trajectories. This model transition section does not satisfy Maxwell's equations, however, and therefore introduces some nonadiabatic behavior in the particle trajectories.

In a cylindrical stellarator field, given above with $k = 0$, some of the basic field structure can be identified analytically. The magnetic field lines migrate about a magnetic axis and ergotically fill a surface, called the magnetic surface. In an $l = 1$ stellarator, the magnetic surfaces are approximately circles near a magnetic axis which helically winds about the geometrical axis. For $l \geqslant 2$ the magnetic axis in a cylindrical stellarator coincides with the geometrical axis of the cylinder. For $l = 2$ the magnetic surfaces near the axis are elliptical, while for $l = 3$ the surfaces have a trefoil shape. Away from the magnetic axis, a separatrix occurs, beyond which the surfaces are no longer closed. As a magnetic field line propagates in the system, it migrates an angle, ι, on the magnetic surface as it moves a distance, $2\pi R$, along the axis. The angle, ι, is the rotational transform, given by

$$\frac{\iota(r)}{2\pi} = \frac{1}{2}\epsilon_l^2 \frac{Rl^3}{r}\frac{d}{dx}\left[\frac{I_l(x)I_l'(x)}{x}\right]$$
$$\simeq \epsilon_l^2\left[\frac{1}{2^l l!}\right]^2 l^5 \alpha R_0 (l\alpha r)^{2(l-2)}\left[(l-1) + \frac{(l\alpha r)^2}{2} + \ldots\right].$$

For $l = 1$ or 2, the rotational transform has a finite value at $r = 0$ and rises slowly with r. For $l \geq 3$, the rotational transform is zero at $r = 0$, and rises faster (higher shear) for larger l as r increases.

The average radius, r_s, of the separatrix for a straight helix is given by

$$l\epsilon_l = \frac{(\alpha r_s)^2}{[1 + (\alpha r_s)^2] I_l(l\alpha r_s)}$$

and the elliptically of the separatrix, for $l = 2$, is given by

$$\text{Ellipticity} = \frac{1 + \epsilon_l}{1 - \epsilon_l}$$

near the magnetic axis. The volume enclosed by the separatrix is the useful volume of th elerator. For $l = 2$, the separatrix radius, r_s, goes to zero as ϵ_l goes to unity.

For high rotational transform, which is needed to concel the particle drifts, a large value of ϵ_l is desired. The radius of the separatrix, however, gives small values of αr_s for ϵ_l near unity, and has no real solution for $\epsilon_l > 1$. The design is therefore a compromise between the need for a large rotational transform and the need for a reasonable volume within the separatrix.

After some trial and error, the design point chosen consists of an $l = 2$ stellarator field with ten helical field periods on a 100 cm radius circle (or $\alpha = 0.1$ cm^{-1}) and $\epsilon_l = 0.7$. This configuration given a rotational transform of $\iota = 5\pi$, and the average separatrix radius is approximately 4 cm, which reasonably utilizes a 5 cm radius drift tube. The ellipticity of the separatrix is 5.7, corresponding to an elliptical minor radius of 3.3 cm and major radius of 4.7 cm for the separatrix.

Figure 2-3 shows the orbit of a 10 MeV test electron in a torus with $R_0 = 100$ cm major radius with $B_0 = 10$ kG, and with no helical field. The particle drifts vertically out of the accelerator volume mainly by curvature drift. When the stellarator field, described above, is included on the torus, the 10 MeV test particle is contained as shown in Fig. 2-4. The 10 MeV electron is approximately the highest energy which can be contained in this configuration. If the guide field strength is doubled to $B_0 = 20$ kG, then a 20 MeV electron trajectory can be contained as shown in Fig. 2-5. The 20 MeV/20 kG trajectory is in fact identical to the 10 MeV/10 kG trajectory.

The scaling of maximum energy with major radius is not linear, as demonstrated by Fig. 2-6, which shows a 23 MeV electron on a 300 cm major radius bend with a guide field, $B_0 = 10$ kG. In this case the number of field periods on the bend was increased to keep the helical pitch length the same as it was in the smaller bend. The 23 MeV trajectory shown is approximately the largest energy which can be contained in this configuration. In each case, the maximum energy is determined by the largest orbit which will fit inside the 5 cm minor radius of the accelerator.

The racetrack configuration has also been tested, and Fig. 2-7 shows a 5 MeV electron which is followed for approximately twenty transits of the accelerator. The particle is well-contained, but its orbit grows slowly during the run, probably due to nonadiabaticity generated in the transition section.

To produce a field model for the racetrack which would not be subject to model-dependent nonadiabatic behavior, the decision was taken to construct the field from an actual surface current distribution. A simple, modular design was achieved in the Tor-2 stellarator in the Soviet Union.[10] Several

other modular stellarator systems have been devised.[11] The Tor-2 system generates an $l = 2$ stellarator field with coils of elliptical cross-section which are rotated relative to each other to produce a helical configuration. By itself this coil design is limited to small values of ϵ_l, since the helical coils will produce a large toroidal field component. A more flexible system consists of surrounding the elliptical coil with a circular coil which carries a current in the opposite sense, thereby partially canceling the toroidal field component due to the elliptical coil. This design has been utilized to construct a modular field coil model for a racetrack stellarator, and avoids the difficulty of analytically modeling the transition section.

The basic scaling laws in energy and fields for a fixed-field racetrack induction accelerator may be summarized as follows:

$E_{MAX} \simeq 1$ MeV/kG For $R_0 = 1$ meter
$E_{MAX} \simeq 2.3$ MeV/kG For $R_0 = 3$ meters

for the accelerator wall located at a minor radius of 5 cm. This configuration, therefore, provides a means of achieving moderate energy performance with a system having no time-dependent fields.

III. HIGH-ENERGY RACETRACK INDUCTION ACCELERATOR

The fixed-field accelerator racetrack requires excessive magnetic field strength to achieve particle energies significantly above 50 MeV in a practical device. It is possible to operate the racetrack as a high-energy induction accelerator (up to 1 GeV) by adding a time-dependent vertical magnetic field to the bends. The vertical field must be made synchronous with the particle energy. The stellarator field now provides an energy bandwidth, which is equivalent to a bandwidth in allowed mismatch of the vertical field and the particle energy. The energy bandwidth is approximately equal to the maximum energy contained in the fixed-field configuration. As the particle accelerates, therefore, the accuracy required for the vertical field to lie within the allowed bandwidth increases.

If the vertical field does not lie in the allowed band, the particle will execute a vertical cross-field drift. In this drift motion the particle will sample radial positions that lie within the Larmor orbit associated with the axial magnetic field. If the vertical field error is small enough that the particle can achieve a new equilibrium position within its Larmor orbit, it will be contained. The accuracy, $\Delta B/B$, required for the vertical magnetic field is thus given by

$$\frac{\Delta B}{B} < \max\left\{\frac{\rho_L}{R}, \frac{\Delta E}{E}\right\}$$

where ρ_L is the Larmor radius, R is the major radius of the bend, ΔE is the energy bandwidth provided by the stellarator field, and E is the particle energy. At high energy, when $\Delta E/E$ becomes small, the Larmor radius becomes large. These criteria combine to permit $\Delta B/B$ in excess of 1% for energies up to nominally 1 GeV.

The vertical magnetic field can be supplied by toroidal windings arranged in a $\cos\theta$ distribution on the toroidal wall in the bends. This configuration provides a vertical magnetic field with high uniformity. A difficult design problem for the racetrack is the termination of these windings where the bends meet the straight sections. In the straight sections, of course, the vertical magnetic field would cause rapid particle loss due to uncompensated drifts. In fact, at each point in the transition from bend to straight the vertical field must cancel the *local* curvature and grad B drifts to high precision.

One approach to this problem is to design the bends with a variable radius of curvature, i.e., not a semicircular bend, so that the local radius of curvature can be matched to the fall-off in the vertical magnetic field. In practice this design would be accomplished by computing the vertical magnetic field for a particular coil and termination configuration, and subsequently calculating the shape required for the bend so that the local magnetic field provides cancellation of the local curvature and grad B drifts.

The vertical magnetic field may be modeled as

$$B_z = B_{z0}\left(1 - n\frac{R - R_0}{r_0}\right)$$

$$B_R = -\, nB_{z0}\,\frac{Z}{R_0},$$

including the vertical field index n, to first-order in the inverse aspect ratio. For the scaling study presented here, the vertical field is assumed uniform ($n = 0$). Runs with finite field index have been made, and give performance which is poorer than the uniform field result.

In the previous section, the stellarator field configuration with $B_0 = 10$ kG was shown to stabilize a one-meter bend for energies up to 10 MeV. The same stellarator field together with a vertical field of 3400 G will contain a 100 MeV electron, as shown in Fig. 3-1. Figures 3-2 and 3-3 demonstrate the results of mismatching the vertical magnetic field for the 100 MeV electron in this configuration. The particle is contained over the vertical field bandwidth given by $3230\ \text{G} \leqslant B_{z0} \leqslant 3570\ \text{G}$.

This bandwidth in B_{z0} is due to the drift cancellation provided by the stellarator field. If the helical field is turned off ($\epsilon_l = 0$), leaving only the toroidal field, $B_0 = 10$ kG, and the vertical field, $B_{z0} = 3230$ G, the 100 MeV test electron drifts vertically out of the torus, as shown in Fig. 3-4.

At an electron energy of 1 GeV, the vertical field for a one-meter bend is approximately 34 kG. This case, therefore, has been studied for a three-meter bend, where the required field is $B_{z0} = 11.367$ kG. The test orbit in this case is shown in Fig. 3-5, for a stellarator field with $B_0 = 10$ kG and with 30 helical field periods on the 3 meter radius circle. Figures 3-6 and 3-7 show the orbits for B_{z0} at the extremes of the bandwidth, $11300\ \text{G} \leqslant B_{z0} \leqslant 11435\ \text{G}$. In this case, the stellarator field is not contributing to the allowed bandwidth.

The scaling law for vertical field and energy for the high-energy racetrack induction linac is

$$B_{z0} = 34\ \text{kG} \cdot \frac{E[\text{GeV}]}{R_0[m]} \cdot \left[1 \pm \alpha\frac{E_{\text{MAX}}}{E}\right]$$

where the first factor, $34\ \text{kG} \cdot E/R_0$, is the required value of B_{z0} to just match the particle energy, E, on a bend of major radius, R_0. The second factor is the bandwidth due to the stellarator field. E_{MAX} is the maximum energy permitted in the fixed-field racetrack induction accelerator (cf., Section 2). The parameter α lies in the range $0.1 \leqslant \alpha \leqslant 1.0$, for $E \leqslant 1$ GeV. As the energy increases, α decreases, so that at 1 GeV the stellarator windings no longer influence the bandwidth.

For electron energy up to several hundred MeV, the high-energy racetrack induction accelerator provides a configuration in which the stellarator field augments the allowed bandwidth of mismatch of vertical field and particle energy. With this augmented bandwidth, it is possible to realize a high-gain acceleration system, using a linear induction accelerator to provide $\gtrsim 1$ MeV/pass.

IV. RACETRACK INDUCTION ACCELERATOR SYSTEM

The utilization of linear induction acceleration technology in a cyclic device implies certain scaling laws for size and weight of the accelerator as functions of beam particle energy. The major scaling laws can be found from a simple system model of the accelerator. This model assumes that all of the volt-seconds of the core are utilized for acceleration, that the bends are stabilized by the combination of solenoidal, helical and vertical fields described in the previous sections, and that the induction module itself is stable to the circulating particle beam. These assumptions about the stability of the device will be discussed in greater detail near the end of this section.

Figure 4-1 shows a schematic drawing of the accelerator system to identify the quantities of interest. Each straight section has length, L, and each bend is assumed to be semi-circle of radius R. Each straight section contains an induction accelerator with total core length, L_c, and core radius, R_c. Particles are assumed to travel at speed, c, the speed of light. The particle transit time, τ, on the racetrack is then

$$\tau = \frac{2L + 2\pi R}{c}.$$

The number of volt-seconds, $V_M T_M$, in the induction modules is given by

$$V_M T_M = 2KR_c L_c.$$

Here, $2R_c L_c$ is the total cross-sectional area of the cores on both legs of the racetrack. The constant, K, is the effective change in magnetic field, ΔB, over the area $2R_c L_c$. The theoretical maximum value of K is 3 Tesla, corresponding to a solid iron core which is swung from $-B_s$ to $+B_s$, where $B_s \approx 1.5$ T is the saturation field for iron. In fact, insulation and packing factors limit the volume of iron in the core, and $K = 1.5$ T will be utilized for this discussion.

The voltage, V_M, is the total energy gain per pass, and may be distributed over several gaps. Four gaps are envisioned, to optimize the core packing factor. One gap would be located at each end of each straight section. The average voltage gradient, g, in the induction accelerator modules is given by

$$V_M = 2gL_c,$$

and the total acceleration time, T_M, is then

$$T_M = \frac{V_M T_M}{V_M} = \frac{KR_c}{g}.$$

At this point, it should be noted that the final particle energy, V, is independent of the gradient g,

$$V = \frac{V_M T_M}{\tau} = \frac{KcR_c L_c}{L + \pi R}.$$

The number of transits, N, required to achieve the particle energy V, does depend on g since

$$N = \frac{T_M}{\tau} = \frac{Kc\ R_c}{2g(L + \pi R)}.$$

The voltage-gain relationship, $\tau = V_M T_M$, that all the volt-seconds be utilized, leads to some interesting scaling laws. This requirement may be written as

$$L + \pi R = \frac{KcR_c L_c}{V}.$$

Since the system is constrained to have $L \geq L_c$ and $R \geq R_c$, i.e., the cores must fit within the racetrack, it is reasonable to examine this system for fixed values of the ratios, R_c/R and L_c/L, as parameters. In this case it is possible to solve for the length, L, as a function of the radius, R, to obtain

$$L = \pi R_0 \frac{R/R_0}{\frac{R}{R_0} - 1},$$

where

$$R_0 \equiv \frac{V}{Kc} \frac{LR}{L_c R_c}.$$

With this relationship between L and R, the transit time, τ, may be expressed as

$$\tau = \frac{2L + 2\pi R}{c} = \frac{2\pi R_0}{c} \frac{(R/R_0)^2}{\frac{R}{R_0} - 1}.$$

This expression is interesting because it yields a *minimum transient time*, τ_M, which thus optimizes the compactness of the system. At the minimum τ, the racetrack is described by

$$\tau_M = \frac{8\pi R_0}{c}$$

$$R = 2R_0$$

$$L = 2\pi R_0.$$

The core dimensions at the minimum τ are given by

$$R_c = \frac{2R_0}{R/R_c}$$

$$L_c = \frac{2\pi R_0}{L/L_c}.$$

The number of volt-seconds is then

$$V_M T_M = 2KR_c L_c = \frac{8\pi}{c}\left(\frac{V^2}{Kc}\right)\left(\frac{RL}{R_c L_c}\right),$$

and the core volume is

$$\text{Vol} = 2\pi R_c^2 L_c = 16\pi^2\left(\frac{V}{Kc}\right)^3\left[\left(\frac{R}{R_c}\right)\left(\frac{L}{L_c}\right)^2\right].$$

Since the main cost of the accelerator is the weight of iron, which is proportional to the core volume, the cost will scale as V^3. These two equations may be used to express the core volume in terms of volt-seconds,

$$\text{Vol} = 16\pi^2\left(\frac{L/L_c}{R/R_c}\right)^{1/2}\left(\frac{V_M T_M}{8\pi K}\right)^{3/2}.$$

The dependence of particle energy, V, with volt-seconds and core volume is shown on Figs. 4-2 and 4-3 for various values of the ratios, R/R_c and L/L_c, and for $K = 1.5$ Tesla, which corresponds to 50% packing of the core volume with iron.

The following table gives the parameters of a racetrack accelerator, which is optimized in the sense that $\tau = \tau_M$, $R = R_c$ and $L = L_c$. The design is for a 200 MeV electron accelerator using $K =$ 1.5 Tesla and $g = 179$ kV/m (corresponding to 1 MeV/pass):

$R = 0.88$ m

$L = 2.8$ m

$V_M T_M = 7.4$ volt-sec

Core Volume $= 13.6$ m^3

$T_M = 7.4\ \mu$s

Beam Energy $= 7.4$ KJ for 1 kA.

The weight of the core in this case would be 51 MT (including the 50% core volume utilization implicit in the value of K). For a 1 kA beam, the capacitor bank required to drive the cores is 15 kJ, corresponding to -50% core losses, which is typical of this type of system.

V. DISCUSSION

Injection into a high current toroidal accelerator is a key problem. The closed field lines of the axial magnetic field that was introduced to contain the space charge of the beam complicates the injector design. A number of experiments have been carried out with varying degrees of success. These include, inductive charging[12-16] magnetic diverters,[17,18] orbit reduction due to self field energy and drift injection.[19]

Electron densities of 10^{10} cm^{-3} ($\sim$100 microcoulombs of charge) have been injected[14] into a magnetic torus by inductive charging. An inductive charging injector is used on the high current betatron experiment[15,16] at U.C. at Irvine.

Magnetic diverters open the toroidal field lines in the region of the injector for a short period of time to allow electrons to enter. A self synchronous scheme[17] which uses the magnetic field produced by the current in the cathode shank of a high current diode to divert field lines has been used successfully. Up to 50% of a 500 kV, 20 kA, 50 μs beam has been injected into a racetrack torus.[18]

The force exerted on the curved field lines of a magnetic torus by a circulating electron beam will cause the beam to drift vertically (perpendicular to the plane of the torus). This drift may be balanced by the addition of a vertical field. This field can be adjusted so that the $\underline{F}_r \times \underline{B}_\phi$ is equal and opposite to the drift resulting from the curved field lines. F_r is the Lorentz force resulting from the azimuthal velocity and vertical magnetic field. If this equilibrium is upset the beam will drift out vertically. Alternatively, by upsetting the equilibrium locally at the edge of the torus, the beam can be drifted into the torus across the field lines. This scheme is attractive for multiturn[19] injection as opposed to the magnetic diverter which is attractive for single turn injection.

The experiments discussed in References 18 and 19 were performed by injecting the beam into neutral gas, rather than at the hard vacuum which is desired for beam acceleration. Parallel injection of a non-neutral beam ring into a toroidal magnetic field in a vacuum has been achieved.[20] A 450 keV, 16 kA, 25 μs beam was injected into a 28 cm major radius torus with a 5.5 cm inner radius. The trapped beam current was 300 A. A quiescent equilibrium that lasted for 20 μs was obtained. The beam made 3000 revolutions around the torus.

The beam was not accelerated in any of the aforementioned experiments. Runaway electrons have been observed in a racetrack stellarator,[7] where the beam is born in the device and is charged neutralized.

These experiments are cited as a partial summary of previous work on injection of high-current beams into closed magnetic configurations. None of this prior experience establishes a solution to the injection problem, which will require a substantial experimental effort. An obvious advantage of the stellarator field configuration is that it allows a large bandwidth in energy mismatch at injection. In addition the externally-improvised rotational transform can be utilized in the injection scheme, since it allows the beam to make many revolutions of the accelerator without returning to the injector. The separatrix associated with the helical field provides additional flexibility in injecting and trapping the electron beam.

The extraction problem, although also untried and nontrivial at high current, may be easier than injection because at a high energy the beam self-field forces are smaller and the effect of the closed toroidal and stellarator fields is reduced. At the final energy the beam responds mainly to changes in the vertical field, which can be perturbed by a kicker. Also, for some applications, it may be reasonable to use the beam in-situ, thereby avoiding the extraction issue altogether.

The high gain and corresponding short acceleration time for the racetrack induction accelerator reduces the impact of synchrotron radiation loss. The energy loss per pass due to synchrotron radiation for a particle of energy, E, in a torus of radius, R_0, is given by

$$P_{\text{sync}} = 88 \frac{E^4[\text{GeV}]}{R_0[m]} \text{ keV/pass.}$$

In a one-meter torus, therefore, a 1 GeV electron will lose 88 keV/pass. The racetrack loses approximately the same energy since the straight sections produce a negligible amount of excess synchrotron radiation loss. Even at 1 GeV in a one-meter bend, the gain per pass, ≥ 1 MeV/pass, in the racetrack far exceeds the energy loss to synchrotron radiation. The short time for acceleration also ensures that the integrated energy loading on the walls due to synchrotron radiation will be negligible.

The discussion of this concept has so far centered on single-particle studies and design issues. In part this emphasis is justified by the need to first establish that a single-particle accelerator configuration can be built to the required energy, i.e., that the proposed device does not require collective effects. In part, though, this study has been structured as it has because of the enormous difficulty associated with generating self-consistent equilibrium and stability analyses in the racetrack field configuration. Nevertheless, some statements on both these subjects can be made.

Self-consistent equilibria and stability of non-neutral systems have been studied in both cylindrical and toroidal geometry for systems with toroidal fields only[21] and for the modified-betatron field configuration.[23] No such study has included the stellarator field structure of the racetrack induction accelerator. The equilibrium studies have found a slow beam drift rotation at the relativistic diocotron frequency, $\omega_d = \omega_p^2/2\gamma^2\omega_c$, where ω_p is the beam plasma frequency, $\omega_p^2 = 4\pi ne^2/\gamma m$, and ω_c is the cyclotron frequency, $\omega_c = eB_0/\gamma mc$ in the toroidal field, B_0. In the simplest approximation, this drift may be regarded as a rigid rotation. The drift arises from the radial force due to the self fields, $-e(E_r - v_z B_\theta/c)$, crossed into the toroidal field. In cylindrical geometry the E_r and B_θ fields are almost equal, $B_\theta = v_z E_r/c$, and the radial force is then given by $-eE_r/\gamma^2$. In toroidal geometry, the fields are modified to first-order in the inverse aspect ratio, and force cancellation to $1/\gamma^2$ does not occur, i.e., residual forces of order, $-eE_r a/R_0$, will exist in a toroidal system even at very high γ.

The same results hold in a stellarator, but are complicated by the elliptical shape of the beam (for $l = 2$). In this case both the beam drift at frequency, ω_d, and the rotational transform due to the helical fields act to move the electrons about the minor axis of the torus. These two motions may either add or subtract, and the performance of the accelerator will probably depend on setting up the helix so that these two effects add constructively. At this point it should be noted that the drift at ω_d does not provide sufficient rotational transform at 10 kA beam strength to operate the accelerator above a few MeV with one-meter bends.

The single-particle trajectory code, described above, may be used to test whether the beam self-fields destroy the accelerator bandwidth. In this case the code is modified to include the beam self-fields as described by Chernin and Sprangle,[22] to first-order in the inverse-aspect ratio. The self-fields are given by

$$B_R^{\text{self}} = -2\pi n_0 e\beta_0 \left[\delta Z + \frac{r_b^2}{a^2}\Delta Z\right]$$

$$B_S^{\text{self}} = 0.$$

$$B_Z^{\text{self}} = 2\pi n_0 \beta_0 \left[\delta R + \frac{r_b^2}{a^2}\Delta R - \frac{r_b^2}{2R_0} l_B\right]$$

$$E_R^{\text{self}} = 2\pi n_0 e \left[\delta R + \frac{r_b^2}{a^2}\Delta R + \frac{r_b^2}{2R_0} l_E\right]$$

$$E_S^{self} = 0.$$

$$E_Z^{self} = -2\pi n_0 e\left[\delta Z + \frac{r_b^2}{a^2}\Delta Z\right],$$

where l_B and l_E are toroidal corrections, given by

$$l_B = 1 + \ln\frac{a}{r_b}$$

$$l_E = \ln\frac{a}{r_b}$$

for a uniform beam current density. The beam center is assumed to be located at coordinates (R_0 + ΔR, ΔZ) and a particular beam particle at ($R_0 + \Delta R + \delta R$, $\Delta Z + \delta Z$) in cylindrical coordinates where Z is the major axis of the torus, R_0 is the major radius of the torus and S is distance measured along the minor axis of the torus. The beam density is n_0, the beam radius is r_b and the beam velocity is $\beta_0 c$ along S.

These fields have been added to the stellarator and toroidal fields described above to include the beam self-field effects in a torus. Figure 5-1a shows the result for a 10 MeV electron in applied fields only and Fig. 5-1b shows the same particle in a 10 kA beam with r_b = 2 cm, with the helix chosen to *add* to the rotational transform due to the beam drift motion in its self-fields. The beam current is seen to have a small beneficial effect on confinement.

The stability of the beam in the racetrack should be good. Stability studies for the modified betatron[23] have shown favorable stability, provided the beam thermal spread is of the order 10% or greater. The stellarator fields induce transverse motion which should provide a strong stabilizing influence. Also, the short acceleration time favors the racetrack stability. Resistive-wall instabilities, for example, are too slow to affect the racetrack accelerator if the wall is a good conductor.

VI. SUMMARY

The high-current racetrack induction accelerator offers several advantages over the other high-current accelerator concepts. Its chief advantage is the high energy gain per pass which is made possible by using linear induction acceleration technology. This feature allows the accelerator to achieve a particular design energy with a short acceleration time, thereby reducing the impact of instabilities and of synchrotron radiation.

The racetrack induction accelerator has several similarities with both the modified betatron and the recirculating linac. It is a high-current, cyclic induction accelerator, like the modified betatron, and it utilizes linear induction accelerator modules, like the recirculating linac. Unlike the modified betatron, however, the racetrack accelerator does not employ a vertical magnetic field for both bending and accelerating the particles. This feature of a betatron configuration forces it to satisfy the flux condition, that the average vertical field enclosed by the orbit equal twice the field at the orbit. On the other hand, the betatron automatically provides synchronization of the vertical field and the particle energy, which must be closely matched at injection. The fixed-field racetrack configuration, at modest energy, requires no synchronization of fields, while the high-energy racetrack must be independently synchronized within a bandwidth of particle energy.

The recirculating linac is a folded linear accelerator in which separate beam channels are passed through the accelerating gap. In this accelerator, the final beam pulse duration is equal to the accelerator pulse length. The racetrack accelerator, on the other hand, delivers a beam pulse of duration equal to the transit time around the circumference of the machine. The recirculating linac provides a large number of accelerated particles at modest energy. Since each particle can only traverse the accelerating

gaps a few times, the recirculating linac must stack accelerators to achieve high energy particles. The racetrack induction accelerator uses the iron to obtain high voltage while the recirculating linac uses the same number of volt-seconds to achieve a long pulse.

In summary, the racetrack induction accelerator offers a new configuration which appears capable of reaching high voltage and high current. This concept extrapolates high-voltage linear induction accelerator technology into the multi-microsecond regime, without sacrificing the high current handling capability of that technology.

The stellarator configuration allows us to design an interesting variation of the betatron or the modified betatron by the addition of strong focussing. The strong focussing makes the accelerator less sensitive to mismatch between magnetic fields and particle energy.

ACKNOWLEDGMENTS

Discussions with S. Penner and M. Wilson of NBS, P. Palmadesso and members of the NRL Advanced Accelerator Project are appreciated. This work was supported by the Office of Naval Research.

REFERENCES

1. C.W. Roberson, IEEE Trans. on Nucl. Sci. **NS-28**, 3433 (1981).

2. P. Sprangle and R.A. Smith, Phys. Rev. A **21**, 293 (1980).

3. R.B. Miller et al., IEEE Trans. on Nucl. Sci. **NS-28**, 3343 (1981).

4. P. Sprangle and C.A. Kapetanakos, J. Appl. Phys. **49**, 1 (1978).

5. G. Barak *et al.*, IEEE Trans. on Nucl. Sci. **NS-28**, 3340 (1981).

6. M.A.D. Wilson, IEEE Trans. on Nucl. Sci. **NS-28**, 3375 (1981).

7. K.M. Young, Plasma Physics **16**, 119 (1974).

8. K. Miyamoto, Nucl. Fusion **18**, 243 (1978).

9. I.S. Danilkin, "Effect of Geometric Errors in the Magnet System on the Field Configuration in a Stellarator," [in *Stellarators*, Proc. of the P.N. Lebedev Physics Inst., D.V. Skobel'tsyn, editor, Consultants Bureau, New York, c. 1974] Vol. 65, pp. 23ff.

10. M.A. Ivanovskii *et al.*, "The Tor-2 Stellarator," [in *Stellarators*, Proc. of the P.N. Lebedev Physics Inst., D.V. Skobel'tsyn, editor, Consultants Bureau, New York, c. 1974] Vol. 65, pp. 61ff.

11. T.K. Chu *et al.*, "Modular Coils: A Promising Toroidal Reactor Coil System," Princeton Plasma Physics Laboratory Report, PPPL-1796 (April, 1981).

12. G.S. Janes, Phys. Rev. Lett. **15**, 135 (1965).

13. J.D. Daugherty, J.E. Eninger, and G.S. Janes, Phys. Fluids **12**, 2677 (1969).

14. W. Clark, P. Korn, A. Mondelli, and N. Rostoker, Phys. Rev. Lett. **37**, 592 (1976).

15. S. Eckhouse, A. Fisher, and N. Rostoker, Phys. Rev. Lett. **42**, 94 (1979).

16. G. Barak *et al., High-Power Beams 81:* Proc. of the 4th Intl. Top. Conf. on High-Power Electron and Ion Beam Research and Technology (Palaiseau, France, June 29-July 3, 1981) Vol. II, pp. 795ff.

17. D.F. Brower, B.R. Kusse, and G.D. Meixel, Jr., IEEE Trans. on Plasma Sci. **PS-2**, 193 (1974).

18. P. Gilad, B.R. Kusse, and T.R. Lockner, Phys. Rev. Lett. **33**, 1275 (1974).

19. J. Benford *et al.*, Phys. Rev. Lett. **31**, 346 (1973); J. Benford, J. Guillory and C. Stallings, J. Appl. Phys. **45**, 1657 (1974); J. Benford, B. Ecker, and V. Bailey, Phys. Rev. Lett. **33**, 574 (1974).

20. A. Mohri, M. Masuzaki, T. Tsuzuki, and K. Ikuta, Phys. Rev. Lett. **34**, 574 (1975).

21. A. Mondelli and N. Rostoker, Proc. Intl. Topical Conf. on Electron Beam Research and Technology (Albequerque, New Mexico, November 3-5, 1975, Sandia Report SAND76-5122) Vol. II, p. 9.

22. D.P. Chernin and P. Sprangle, "Transverse Beam Dynamics in the Modified Betatron," NRL Memorandum Report 4687 (1982).

23. P. Sprangle and J. Vomvorides, "Longitudinal and Transverse Instabilities in a High Current Modified Betatron Electron Accelerator," NRL Memorandum Report 4688 (1981).

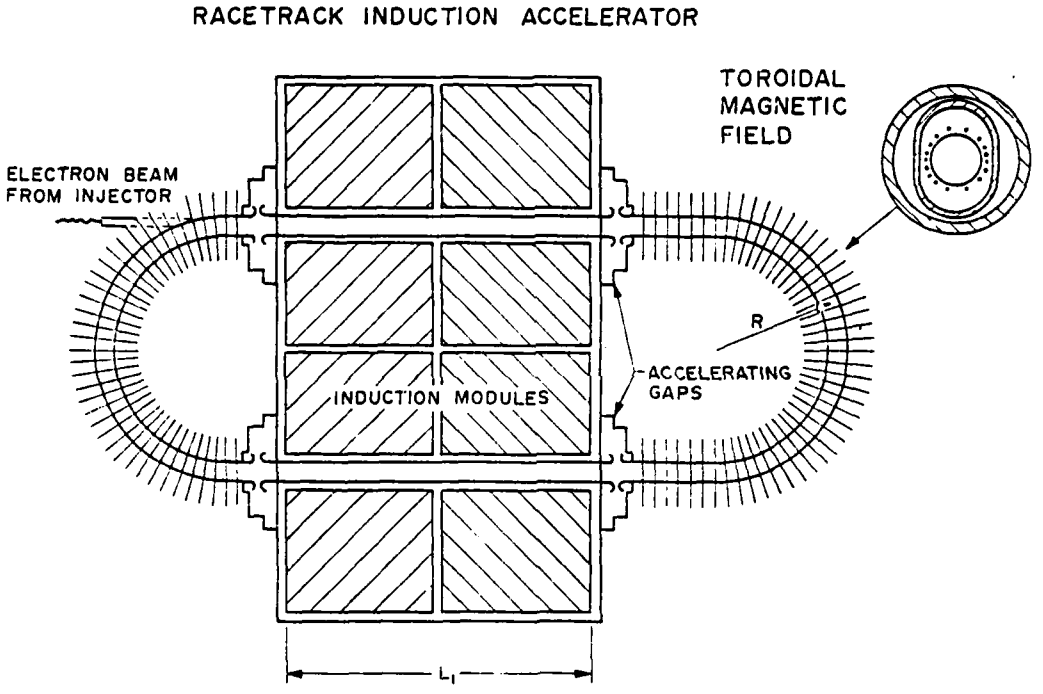

Fig. 1-1 — Schematic of Racetrack Induction Accelerator. Inset shows cross-section of the field coils which generate toroidal, helical and vertical magnetic fields in the bends.

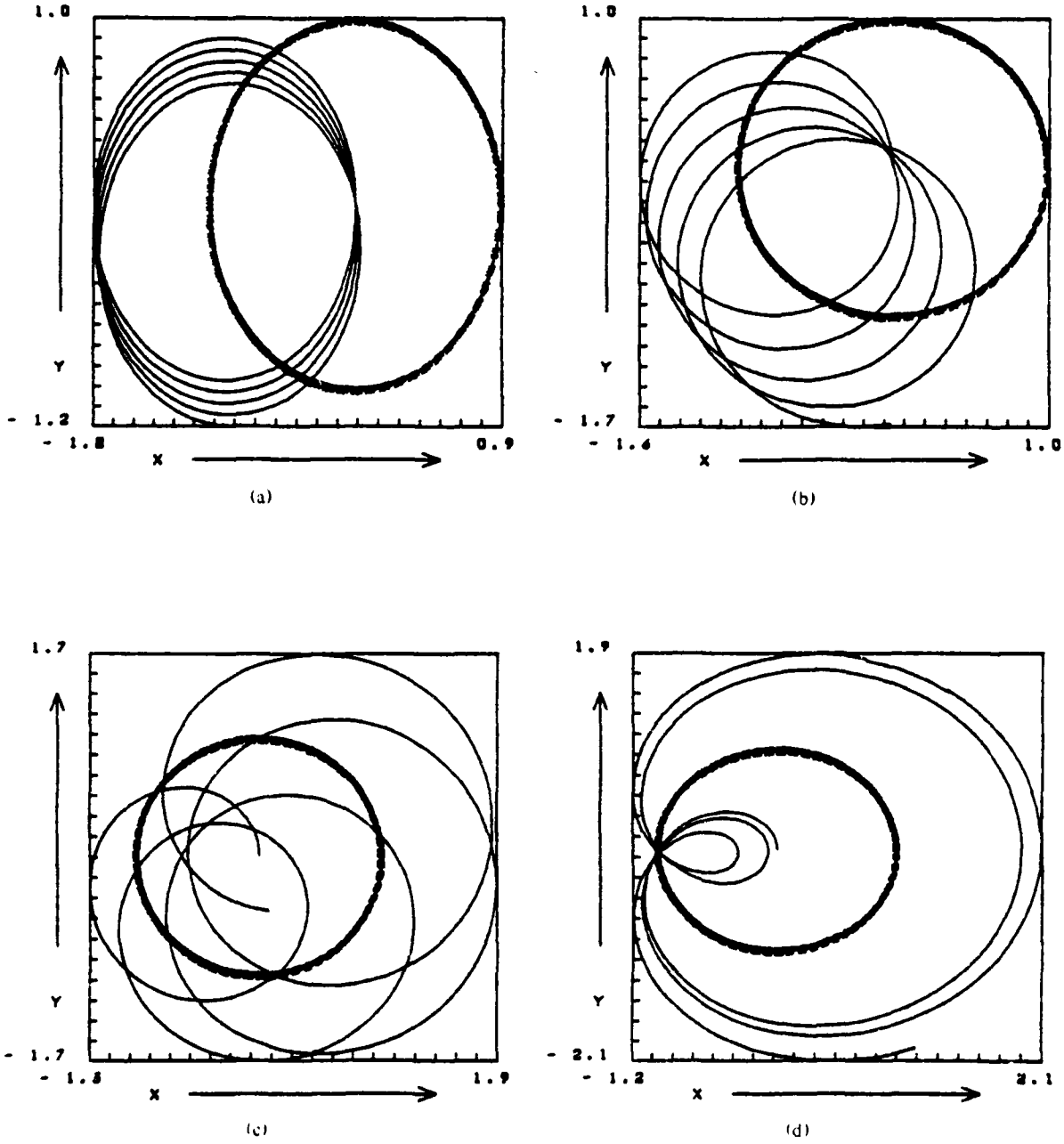

Fig. 1-2 — Single-particle drift orbits for a cylindrical helix. The heavy curve is the equilibrium orbit. Curves are for $\bar{\eta} = -.001$ and $\bar{\beta}$ varied from 0.1 to 0.5.

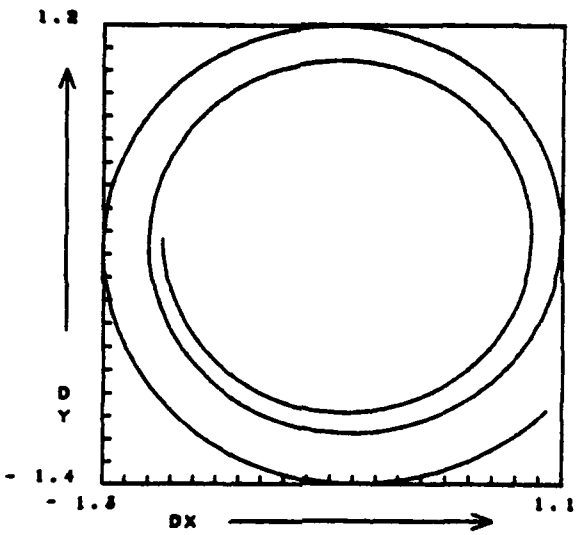

Fig. 2-2 — Single-particle drift orbit displacement from equilibrium, δx vs δy, for $\tilde{\beta} = 0.5$

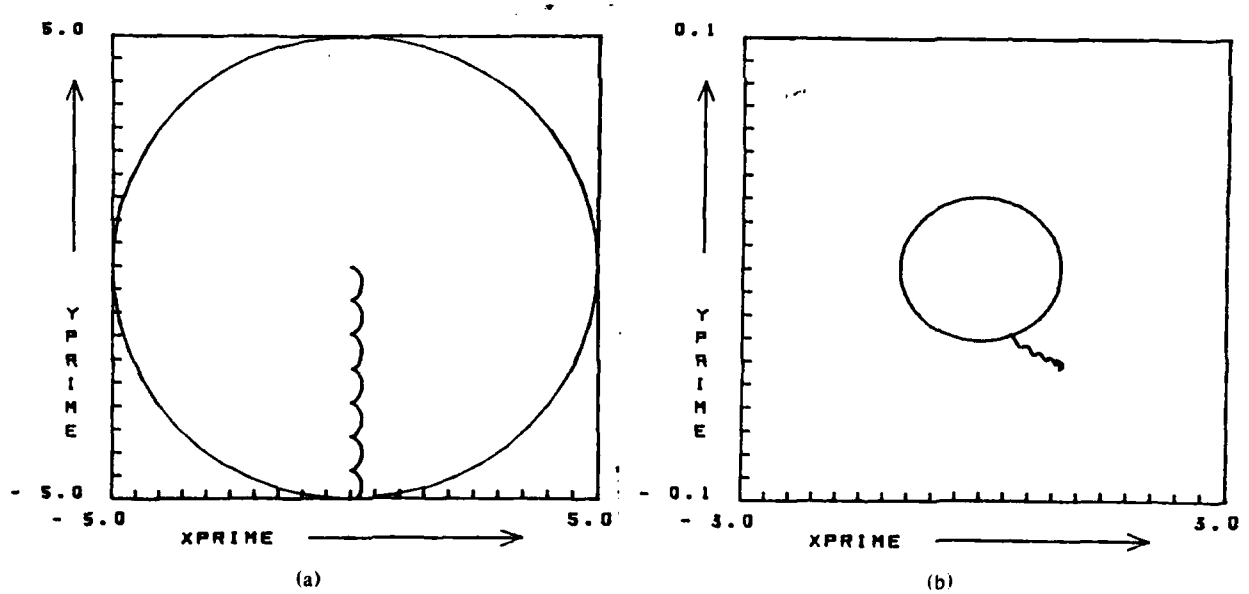

Fig. 2-3 — 10 MeV test electron trajectory on a 1 meter bend with a 10 kG toroidal guide field, showing (a) minor cross-section projection and (b) global projection

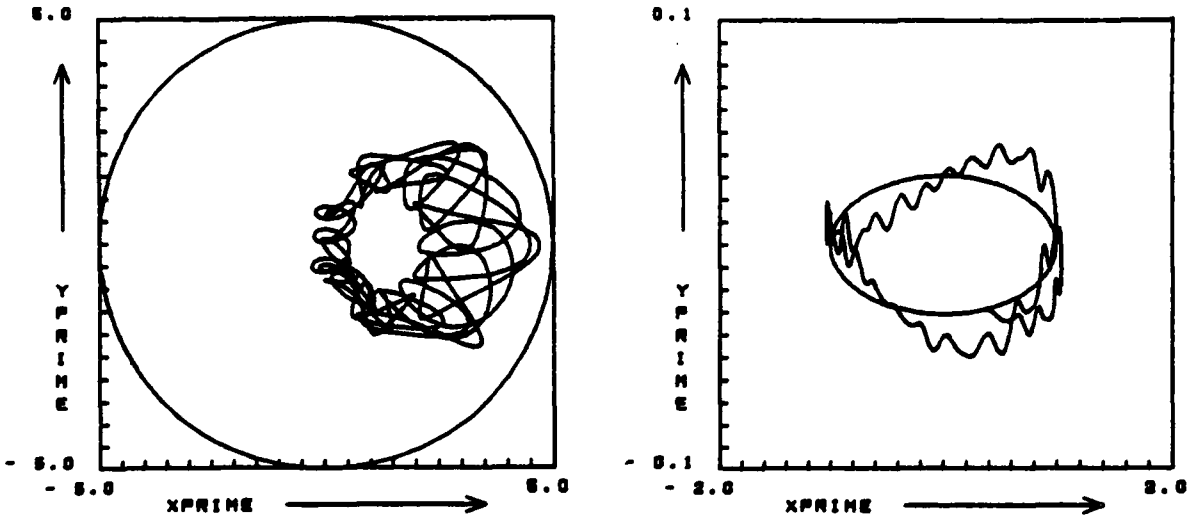

Fig. 2-4 — Same as Fig. 2-3 with addition of an $l = 2$ helical field with $spsilon_l = 0.7$ and 10 helical field periods around the full torus

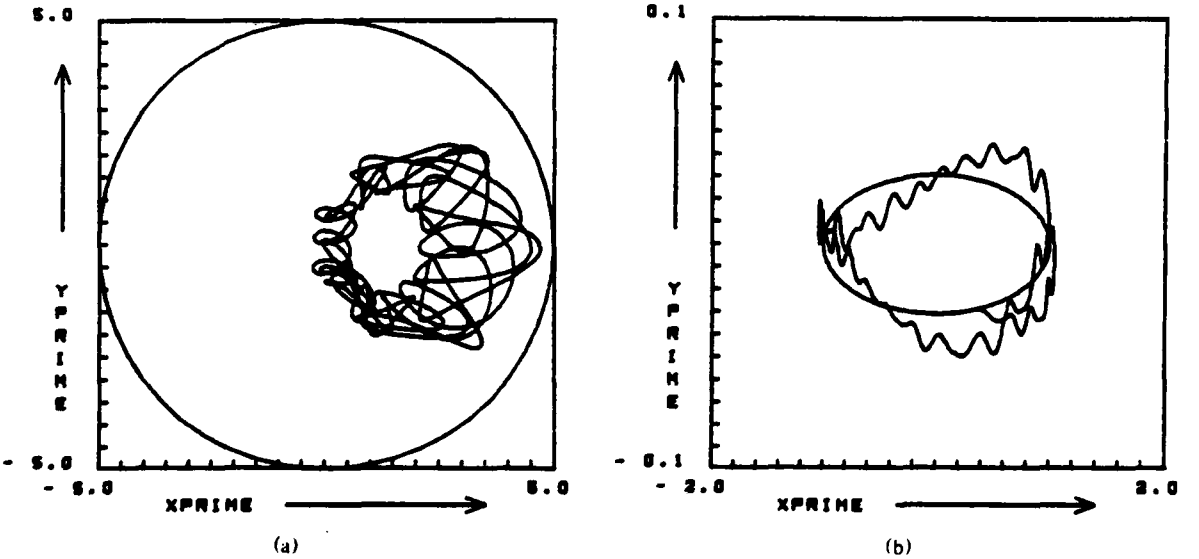

Fig. 2-5 — 20 MeV test electron trajectory on a 1 meter bend with a 20 kG toroidal guide field plud $l = 2$ helical field having $\epsilon_l = 0.7$ and 10 helical periods in $2\pi R$

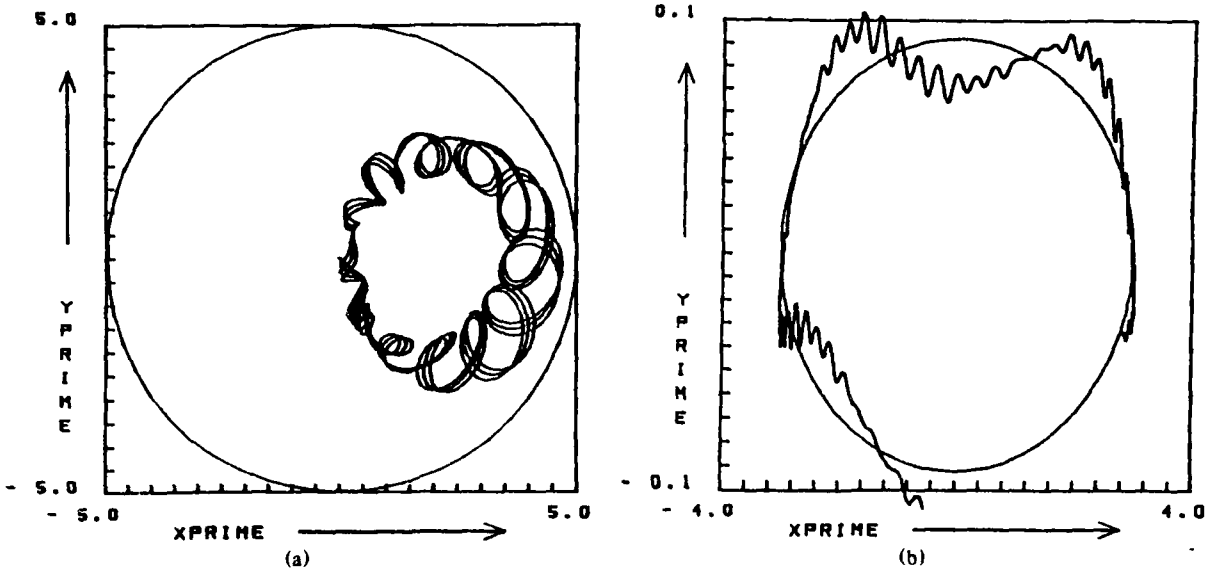

Fig. 2-6 — 23 MeV test electron trajectory on a 3 meter bend with a 10 kG toroidal guide field plus $l = 2$ helical field having $\epsilon_l = 0.7$ and 30 helical periods in $2\pi R$

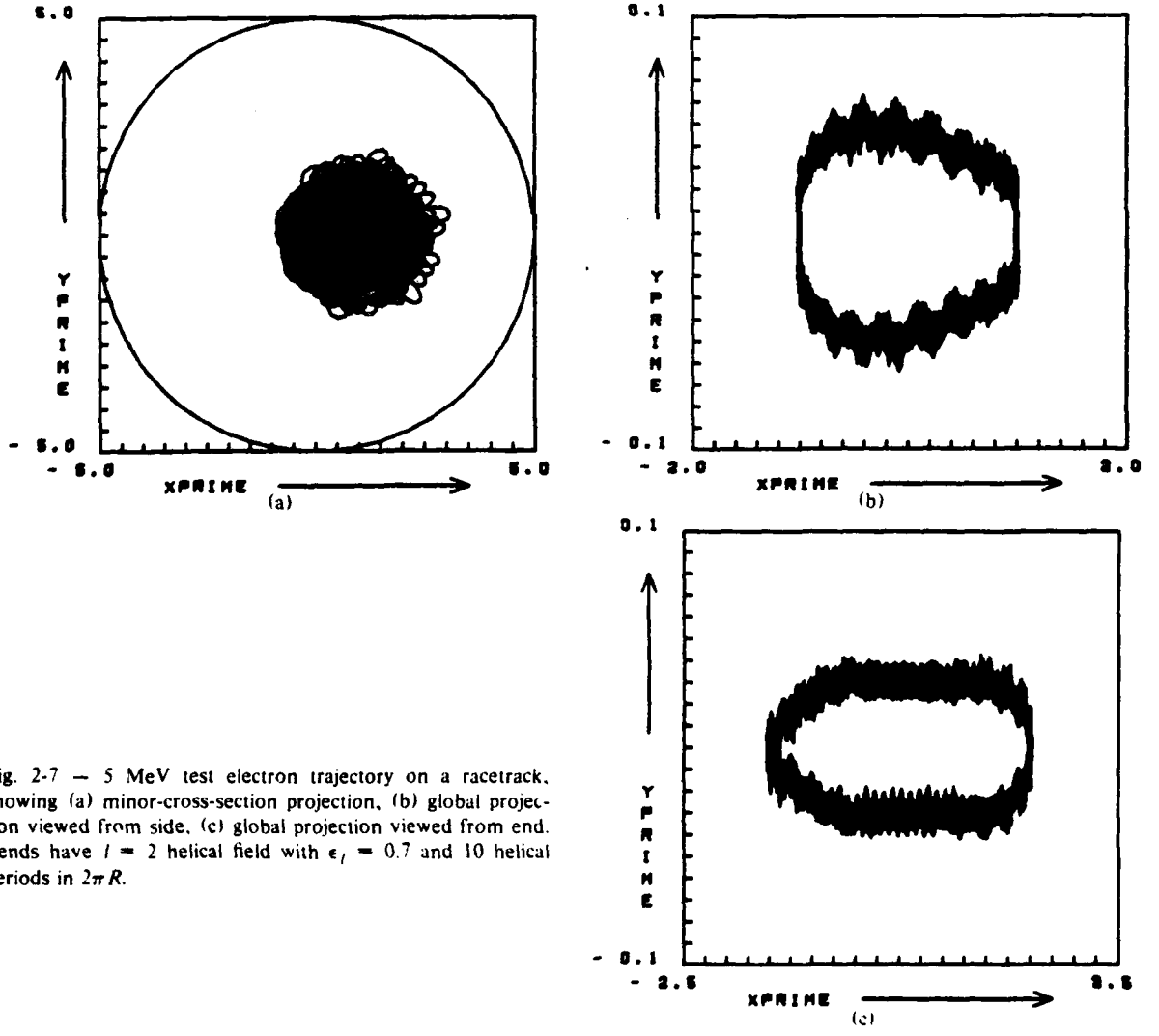

Fig. 2-7 — 5 MeV test electron trajectory on a racetrack, showing (a) minor-cross-section projection, (b) global projection viewed from side, (c) global projection viewed from end. Bends have $l = 2$ helical field with $\epsilon_l = 0.7$ and 10 helical periods in $2\pi R$.

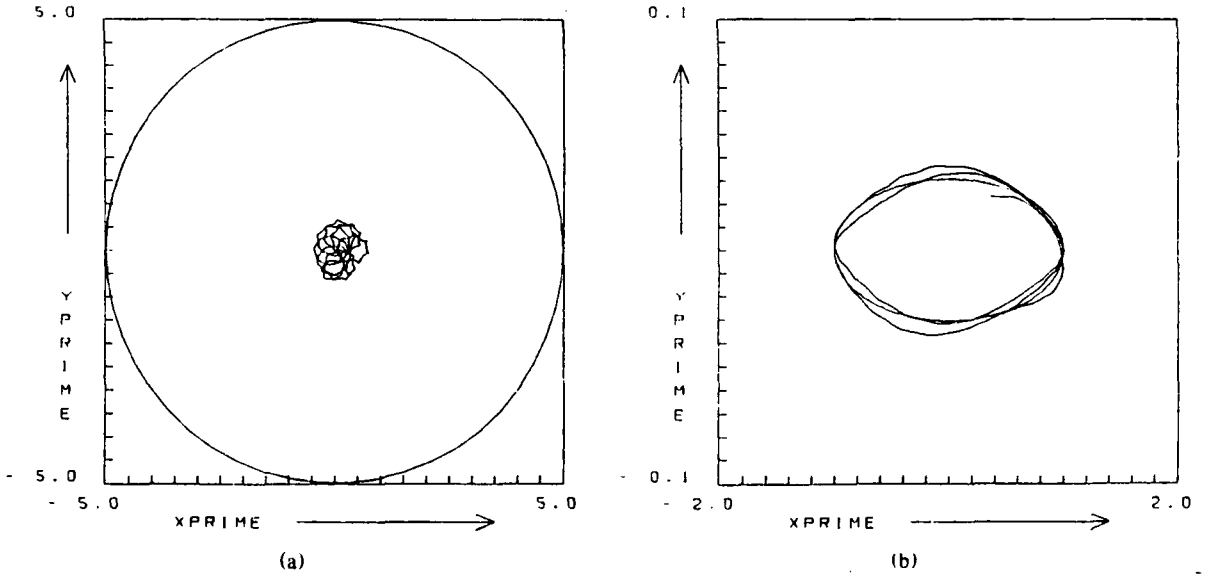

Fig. 3-1 — 100 MeV test electron trajectory on a 1 meter bend with 10 kG toroidal guide field plus $l = 2$ helical field with $\epsilon_l = 0.7$ and 10 helical field periods in $2\pi R$ plus vertical magnetic field of 3400 gauss

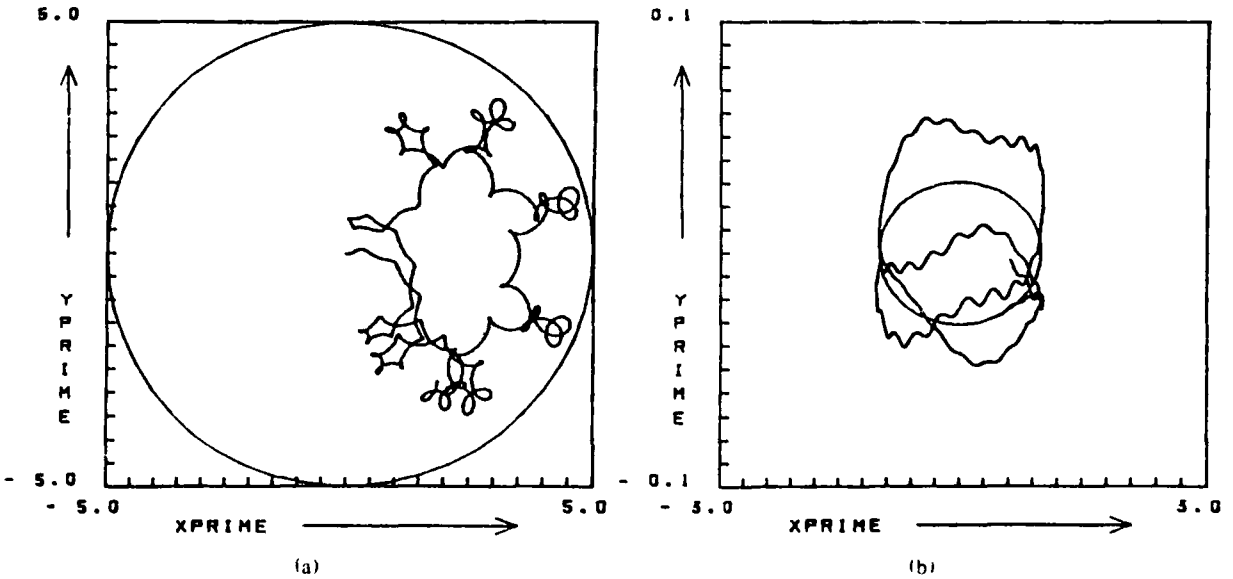

Fig. 3-2 — Same as Fig. 3-1, except vertical magnetic field is 3230 gauss

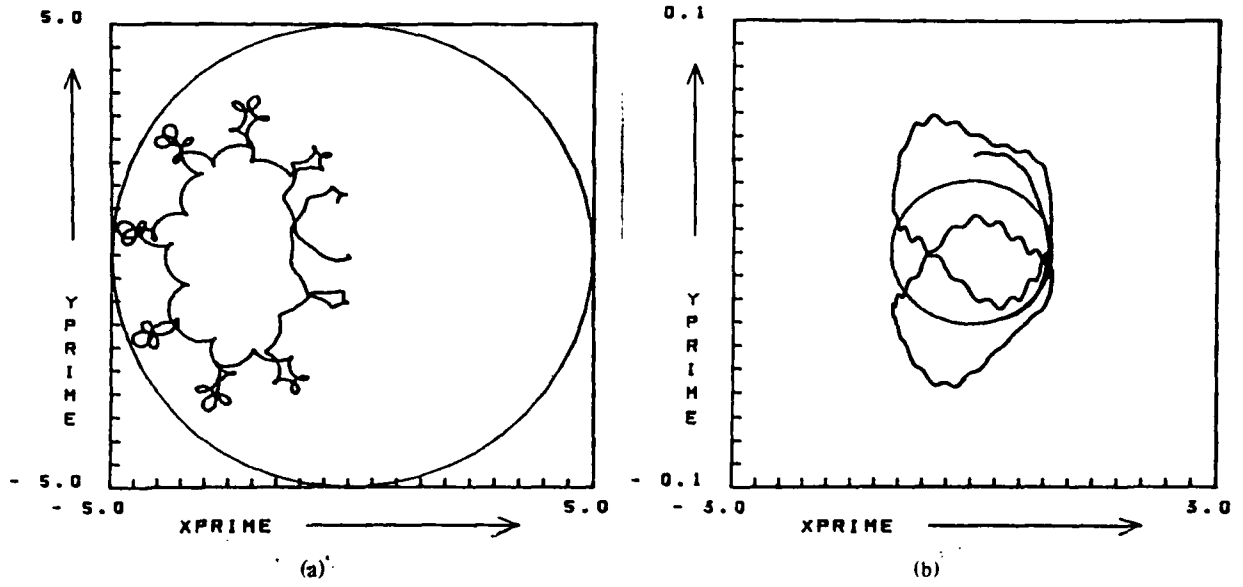

Fig. 3-3 — Same as Fig. 3-1, except vertical magnetic field is 3570 gauss

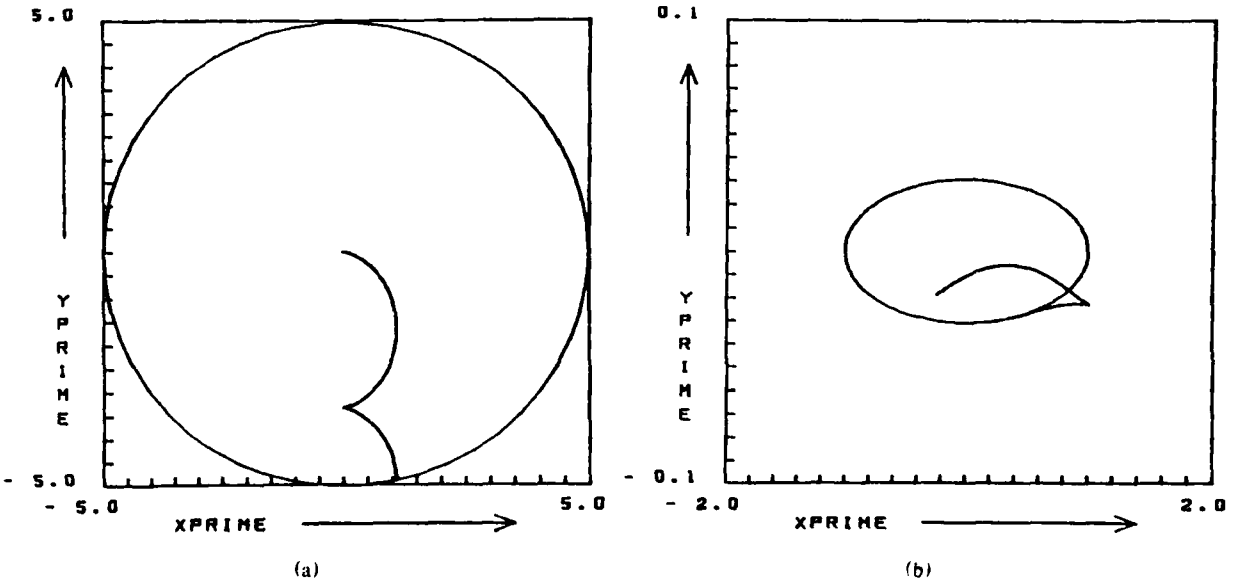

Fig. 3-4 — Same as Fig. 3-2, except helical field is zero

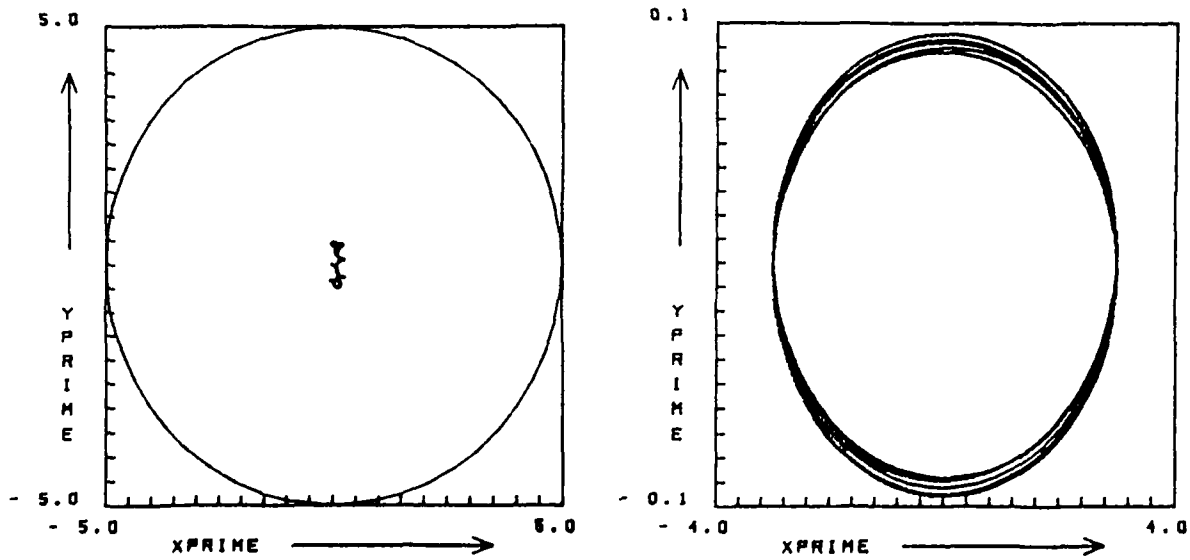

(a) (b)

Fig. 3-5 — 1 GeV test electron trajectory on a 3 meter bend with 10 kG toroidal field plus $l = 2$ helical field with $\epsilon_l = 0.7$ and 30 helical periods in $2\pi R$ plus vertical magnetic field of 11.367 kG

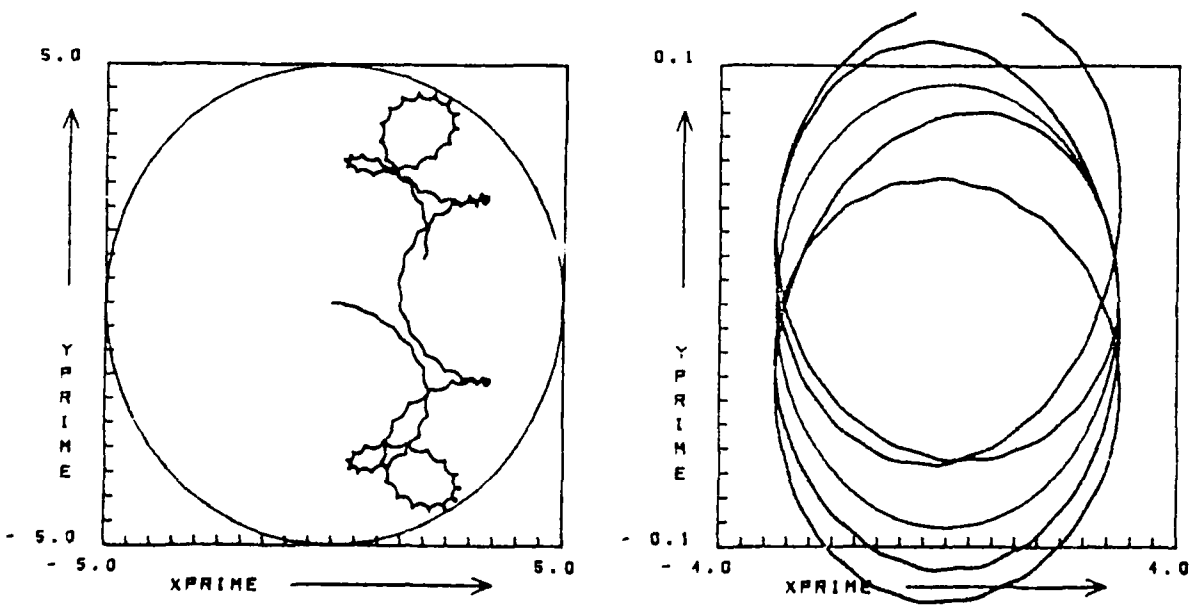

(a) (b)

Fig. 3-6 — Same as Fig. 3-5, except vertical magnetic field is 11.300 kG

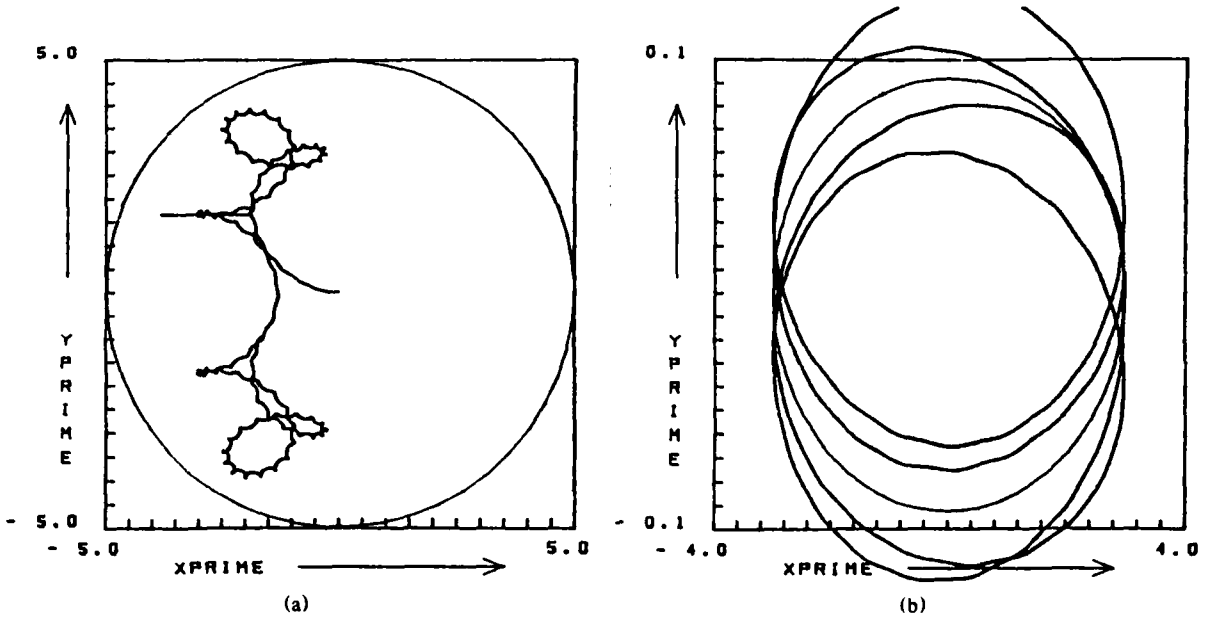

Fig. 3-7 — Same as Fig. 3-5, except vertical magnetic field is 11.435 kG

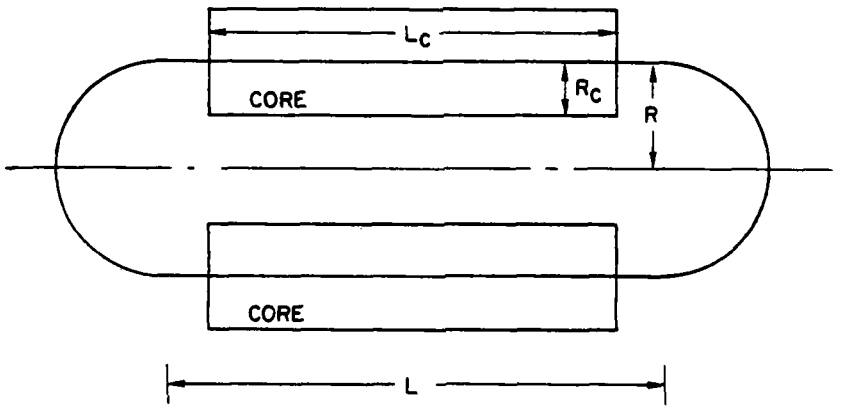

Fig. 4-1 — Schematic drawing of accelerator for system scaling study

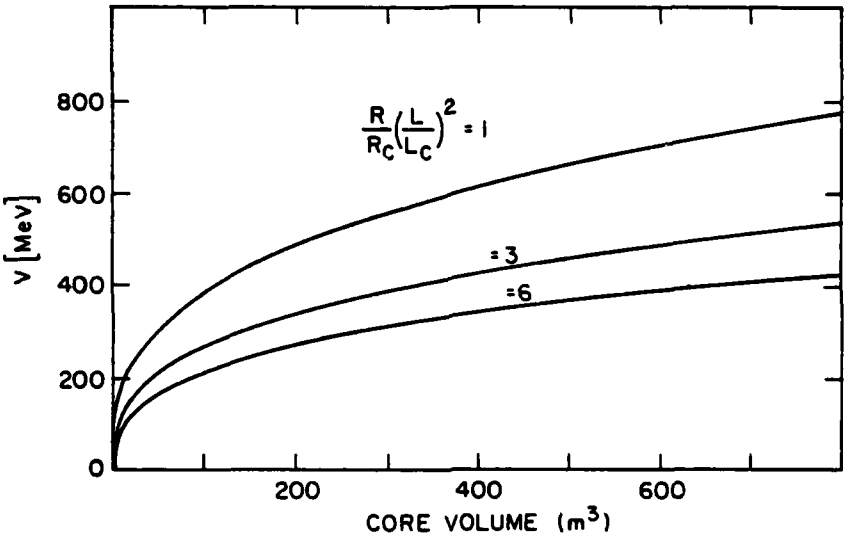

Fig. 4-2 — Final particle energy vs core volume

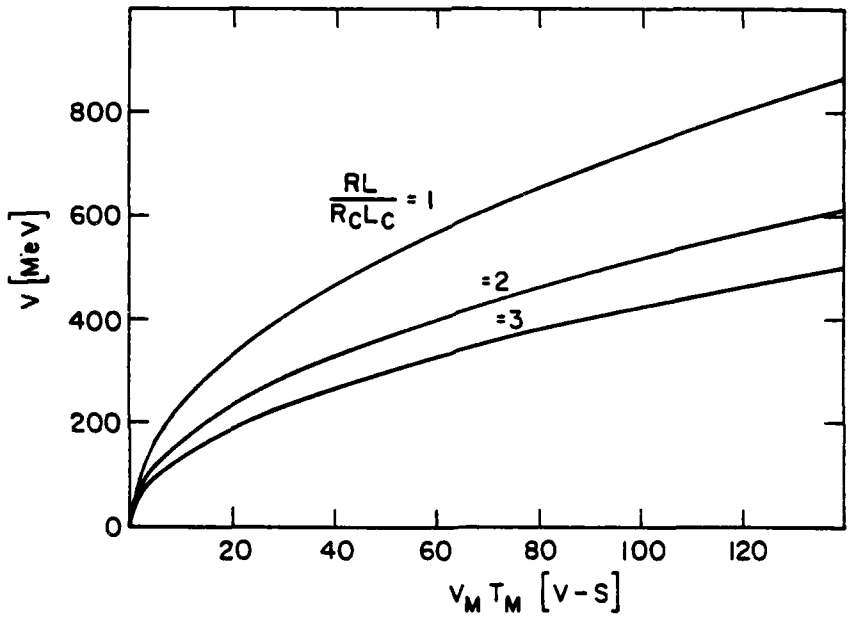

Fig. 4-3 — Final particle energy vs volt-seconds in cores

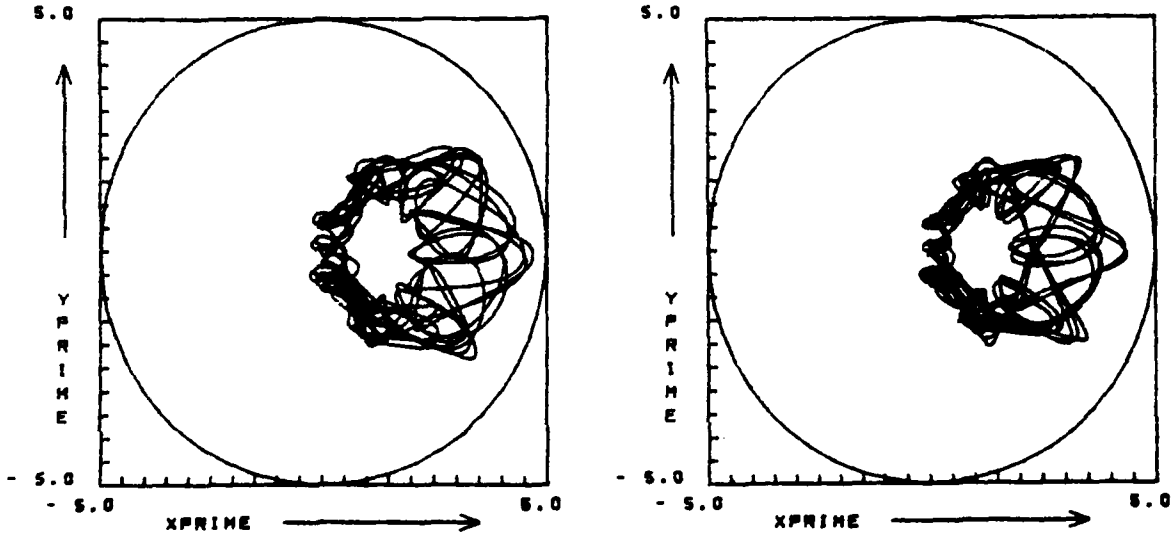

Fig. 5-1 — Effect of beam self-fields on 10 MeV test electron trajectory on a 1 meter bend with 10 kG toroidal field plus $l = 2$ helical field with $\epsilon_l = 0.7$ and 10 helical field periods in $2\pi R$

(a) No beam — same as Fig. 2-4

(b) $I_b = 10$ kA, $r_b = 2$ cm beam centered at $\Delta R = 1.0$ cm, $\Delta z = 0$ self-fields included

END

FILMED

2-83

DTIC